Phosphorylation-Dependent Assembly of a 14-3-3 Mediated Signaling Complex During Red Blood Cell Invasion by *Plasmodium falciparum* Merozoites

Kunal R. More[a], Inderjeet Kaur[b], Quentin Giai Gianetto[c,d], Brandon M. Invergo[e,f], Thibault Chaze[c], Ravi Jain[g], Christéle Huon[a], Petra Gutenbrunner[f], Hendrik Weisser[f], Mariette Matondo[c], Jyoti S. Choudhary[f], Gordon Langsley[h], Shailja Singh[a,g*] and Chetan E. Chitnis[a,b*]

[a] Malaria Parasite Biology and Vaccines Unit, Department of Parasites and Insect Vectors, Institut Pasteur, Paris, France

[b]International Centre for Genetic Engineering and Biotechnology (ICGEB), New Delhi, India

[c]Proteomics Platform, Mass Spectrometry for Biology Unit, USR CNRS 2000, Institut Pasteur, Paris, France

[d]Bioinformatics and Biostatistics HUB, Computational Biology Department, USR CNRS 3756, Institut Pasteur, Paris, France

[e]EMBL-European Bioinformatics Institute, Wellcome Genome Campus, Hinxton, UK

[f] Proteomic Mass Spectrometry Group, Wellcome Trust Sanger Institute, Hinxton, UK

[g]Special Centre for Molecular Medicine, Jawaharlal Nehru University, New Delhi, India

[h]Institut Cochin, Inserm U1016, Paris, France

Running title: Signaling complex during merozoite invasion

Abstract: 232 words; Text: 5494 words

*Address correspondence to: Chetan E. Chitnis, chetan.chitnis@pasteur.fr; or Shailja Singh, shailjasngh@gmail.com

Abstract

Red blood cell (RBC) invasion by *Plasmodium* merozoites requires multiple steps that are regulated by signaling pathways. Exposure of *P. falciparum* merozoites to the physiological signal of low K^+, as found in blood plasma, leads to a rise in cytosolic Ca^{2+}, which mediates microneme secretion, motility, and invasion. We have used global phosphoproteomic analysis of merozoites to identify signaling pathways that are activated during invasion. Using quantitative phosphoproteomics we found 394 protein phosphorylation site changes in merozoites subjected to different ionic environments (high K^+/ low K^+) out of which 143 were Ca^{2+}-dependent. These included a number of signaling proteins such as catalytic and regulatory subunits of protein kinase A (PfPKAc and PfPKAr) and calcium-dependent protein kinase 1 (PfCDPK1). Proteins of the 14-3-3 family interact with phosphorylated target proteins to assemble signaling complexes. Here, using co-immunoprecipitation and gel filtration chromatography, we demonstrate that Pf14-3-3I binds phosphorylated PfPKAr and PfCDPK1 to mediate the assembly of a multi-protein complex in *P. falciparum* merozoites. A phospho-peptide, P1, based on the Ca^{2+} dependent phosphosites of PKAr, binds Pf14-3-3I and disrupts assembly of the Pf14-3-3I-mediated multi-protein complex. Disruption of the multi-protein complex with P1 inhibits microneme secretion and RBC invasion. This study thus identifies a novel signaling complex that plays a key role in merozoite invasion of RBCs. Disruption of this signaling complex could serve as a novel approach to inhibit blood stage growth of malaria parasites.

Importance

Invasion of red blood cells (RBCs) by *Plasmodium falciparum* merozoites is a complex process that is regulated by intricate signaling pathways. Here, we have used phosphoproteomic profiling to identify the key proteins involved in signaling events during invasion. We found changes in the phosphorylation of various merozoite proteins including multiple kinases previously implicated in the process of invasion. We also found that a phosphorylation dependent multi-protein complex including signaling kinases assembles during the process of invasion. Disruption of this multi-protein complex impairs merozoite invasion of RBCs providing a novel approach for the development of inhibitors to block the growth of blood stage malaria parasites.

Introduction

The clinical symptoms of *Plasmodium falciparum* malaria are attributed to the blood stage of the parasite life cycle during which merozoites invade and multiply within host red blood cells (RBCs). Following the development of mature schizonts, newly formed merozoites egress and invade uninfected RBCs to initiate a new cycle of infection. The invasion of RBCs by *P. falciparum* merozoites is a complex multi-step process that is mediated by specific molecular interactions between red cell surface receptors and parasite protein ligands (1). These ligands are initially located in internal secretory organelles called micronemes and rhoptries and are released to the merozoite surface in tightly regulated steps (2).

Exposure of merozoites to a low potassium (K^+) environment in blood plasma initiates a signaling cascade that involves second messengers like Ca^{2+} and cyclic nucleotides that activate effector molecules such as kinases and phosphatases (3-5). These effectors modulate phosphorylation of target proteins to activate merozoite motility, as well as secretion of invasion related proteins such as *P. falciparum* 175 kD erythrocyte binding antigen (PfEBA175) and apical merozoite antigen-1 (PfAMA1) from the micronemes to the merozoite surface (2). The engagement of PfEBA175 with its receptor glycophorin A triggers another signaling cascade that leads to the release of rhoptry proteins such as PfRH2b (5). The secretion of microneme and rhoptry proteins seals the engagement of the merozoite with the RBC and enables completion of the invasion process.

The signaling mechanisms that regulate processes such as apical organelle secretion and merozoite motility during host cell invasion are not fully understood. Protein phosphorylation is known to be the primary regulator of biological signaling pathways and phosphoproteome analysis can provide information about the signaling pathways that are activated in a cell in response to different stimuli (6). Protein phosphorylation/dephosphorylation acts as a molecular switch that can lead to diverse outcomes including activation or deactivation of enzymes, preparation of proteins for degradation, translocation of proteins to various cellular compartments and establishment of protein-protein

interactions leading to the formation of multi-protein complexes that function in signaling pathways (7).

Phosphorylation-dependent formation of multi-protein signalling complexes plays a key role in the regulation of diverse cellular processes (8-10). For example, in human cells, phosphorylation of membrane-associated guanylate kinase-like domain-containing protein (CARMA) by protein kinase C (PKC) leads to the formation of CARMA1-Bcl10-MALT1 (CBM) complex, which activates the transcription factor NF-κB to regulate cell survival, activation and proliferation (8). A family of scaffold proteins, referred to as the 14-3-3 family, binds phosphorylated proteins to assemble signaling complexes in diverse systems (9-10). For example, in the brain, a 14-3-3ζ dimer simultaneously binds and bridges the cytoskeletal protein tau and glycogen synthase kinase, GSK3β, to stimulate tau phosphorylation, which in turn regulates microtubule dynamics (9). In the case of *Arabidopsis thaliana*, calcium-dependent phosphorylation of a basic region/leucine-zipper (bZIP) transcription factor FD leads to the formation of a florigen complex with flowering locus T protein that is mediated by 14-3-3 and regulates flowering (10). Phosphorylation analysis of *P. falciparum* schizont stages also reported the formation of a phosphorylation-dependent high-molecular-weight complex involving calcium-dependent protein kinase-1 (PfCDPK1) (11), although the precise composition of the complex was not defined.

In this study, we present a phospho-protein profile of *P. falciparum* merozoites and identify signal-dependent phosphorylation events that play important roles in the RBC invasion process. Importantly, we describe the formation of a phosphorylation-dependent, dynamic, high-molecular-weight complex involving PfCDPK1 and PfPKAr and explore the role of Pf14-3-3 in the assembly of this complex. Disruption of the Pf14-3-3-mediated protein complex with a peptide mimic inhibits RBC invasion by merozoites providing a novel strategy to block blood stage growth of malaria parasites.

Results

Phosphoproteome analysis of *P. falciparum* merozoites. Merozoites released from synchronized *P. falciparum* schizonts were purified (5) and processed for mass-spectrometric phosphoproteome analysis. The workflow used for phosphoproteomics and data analysis are outlined in Figure S1. Dataset S1 provides the list of phosphorylated proteins and phosphosites identified in *P. falciparum* merozoites. Comparison with the published *P. falciparum* merozoite phosphoproteome (12) identified 2786 phosphosites and 666 merozoite phosphoproteins that are unique to our study (Fig. 1a). Potential protein-protein interactions in the merozoite phosphoproteome are illustrated as MCODE clusters (Fig. S2 and Dataset S2). Enriched in MCODE cluster 1 are 132 proteins relevant to host cell invasion (Fig. 1b). The phosphorylated proteins in MCODE cluster 1 include signaling related proteins such as Protein Kinase G (PfPKG; PF3D7_1436600), Guanylate Cyclase (PfGC; PF3D7_1138400), Protein Kinase A regulatory subunit (PfPKAr; PF3D7_1223100), Protein Kinase A catalytic subunit (PfPKAc; PF3D7_0934800), Calcium Dependent Protein Kinase 1 (PfCDPK1; PF3D7_0217500) and Calcium-Dependent Protein Phosphatase Calcineurin (PfCNA; PF3D7_0802800) as well as invasion related parasite proteins such as merozoite surface protein-1 (MSP1), erythrocyte binding antigens (EBA181, EBA140) rhoptry neck proteins (RON2, RON3, RON4) and parasite proteins responsible for motility such as GAP45, GAP40, MyoA, MyoB and MTIP (Fig. 1b). The presence of both calcium and cyclic nucleotide responsive effectors in MCODE cluster 1 (Fig. 1b) indicates significant crosstalk between these second messengers at the time of invasion.

Exposure of *P. falciparum* merozoites to an ionic environment mimicking blood plasma induces changes in protein phosphorylation. We have shown previously that merozoites respond to changes in their ionic environment, especially changes in potassium ion (K^+) concentration (5). Exposure of merozoites to a low K^+ environment, which is characteristic of extracellular ionic conditions in blood

plasma, serves as a signal to trigger a rise in Ca^{2+} and cAMP, which activates signaling cascades (4, 5). We performed quantitative phosphoproteomics on merozoites resuspended in buffers mimicking intracellular and extracellular ionic conditions (IC buffer and EC buffer) to identify differences in protein phosphorylation. This resulted in the identification of 1499 unique phosphosites corresponding to 587 *P. falciparum* proteins (Dataset S3). Ca^{2+}-dependent changes in phosphorylation were identified by studying differences in phosphorylation of merozoite proteins in IC buffer compared to either EC buffer or EC buffer + BAPTA-AM (EC-BA) (Dataset S3).

Proteins exhibiting statistically significant fold changes in phosphorylation at specific amino acid residues in merozoites in EC buffer compared to IC buffer and in EC-BA buffer compared to IC buffer were identified. Peptides from the same proteins without any phosphorylation were quantified and used to normalize for differences in concentration of proteins in merozoite samples under different conditions. Based on results of two independent biological replicates with each replicate analyzed two times by mass spectrometry, we identified 394 phosphoresidues as significantly altered when merozoites are exposed to EC buffer compared to IC buffer. Of these, phosphorylation at 143 sites is blocked by Ca^{2+} chelator, BAPTA-AM (Datasets S3 and S4). Changes in phosphorylation of some key signaling related proteins such as PfPKA-R, PfCDPK1 and Pf14-3-3I were observed (Figs. 2a, 2b). Phosphorylation of PfCDPK1 on Ser 28/34, and Ser 64 was significantly upregulated in merozoites exposed to EC buffer as compared to IC buffer (Fig. 2a, 2c). Chelation of Ca^{2+} with BAPTA-AM had no effect on these phosphorylation events (Fig. 2b, 2c). Phosphorylation on Ser 17 and Ser 217 of PfCDPK1 was found to be higher in merozoites in EC-BA buffer compared to IC buffer. However, there was no increase in phosphorylation of Ser 17 and Ser 217 in EC buffer compared with IC buffer (Fig. 2c). In contrast, phosphorylation of PfPKAr in EC buffer at Ser 113/Ser 114 was dependent on the presence of Ca^{2+} (Fig. 2d). Corresponding spectra and quantification profile for phosphorylation of PfCDPK1 on Ser 28/34 and of PfPKAr on Ser 113/Ser 114 are represented in Fig. S3. PfCDPK1 and

158 PfPKAr are known to be involved in RBC invasion by merozoites (4,13). We, therefore, investigated
159 further the relevance of changes in their phosphorylation status to the process of invasion.

160 The changes in phosphorylation of key signaling proteins, PfCDPK1, PfPKAr and Pf14-3-3I, in
161 EC buffer compared to IC buffer were also confirmed using anti-phosphoserine antibodies. Lysates of
162 *P. falciparum* merozoites in IC and EC buffers were used for IP with anti-PfCDPK1 and anti-PfPKAr
163 sera. The IPs were separated by SDS-PAGE and PfCDPK1 and PfPKAr were detected by western
164 blotting. The blots were also probed with anti-phosphoserine antibodies to determine levels of serine
165 phosphorylation in these proteins (Fig. S4a). Western blotting with anti-phosphoserine antibodies
166 confirmed that the levels of phosphorylated serines in PfCDPK1 and PfPKAr were higher in EC buffer
167 compared to IC buffer (Fig. S4a). Moreover, each IP sample showed multiple proteins with increased
168 serine phosphorylation suggesting that these phosphorylated proteins may interact with each other to
169 form a multi-protein complex.

170

171 **Formation of a multi-protein complex involving PfPKAr, PfCDPK1and Pf14-3-3I in *P. falciparum***
172 **merozoites.** To investigate the interactions of signaling proteins, PfPKAr and PfCDPK1, in merozoites,
173 we immunoprecipitated PfPKAr and PfCDPK1 from merozoite lysates using specific polyclonal sera
174 and identified interacting proteins in the IPs by mass spectrometry. The presence of PfPKAr in IPs with
175 anti-PfCDPK1 sera was confirmed by detection of multiple PfPKAr peptides with greater than 50%
176 sequence coverage (Table 1). Similarly, presence of PfCDPK1 is confirmed in IPs performed with anti-
177 PfKAr sera. Multiple PfCDPK1 peptides, with greater than 50% sequence coverage, are detected in IPs
178 performed with anti-PfPKAr sera (Table 1). In addition, the scaffold protein, Pf14-3-3I, is also detected
179 in IPs performed with both anti-PfCDPK1 and anti-PfPKAr sera with multiple Pf14-3-3I peptides
180 detected that provide greater than 50% sequence coverage. The presence of Pf14-3-3I in the complex is
181 further confirmed by detection of PfCDPK1 and PfPKAr peptides with greater than 50% sequence

coverage in IPs performed with anti-Pf14-3-3I sera (Table 1). These studies suggest that Pf14-3-3I, PfCDPK1 and PfPKAr interact to form a multi-protein complex in *P. falciparum* merozoites (Table 1). In addition to PfPKAr, PfCDPK1 and Pf14-3-3I, four other proteins (elongation factor 1-alpha, glyceraldehyde-3-phosphate dehydrogenase (GAPDH), phosphoethanolamine N-methyltransferase (PMT), actin-depolymerizing factor 1 (ADF1)) were detected at similar stringency levels in IPs with all three sera, (anti-PfPKAr, anti-PfCDPK1 and anti-Pf14-3-3I sera) (Dataset S5). A number of other proteins are detected at lower stringency in the IPs by mass spectrometry (Dataset S5). As a negative control for specificity, we used specific antisera to *P. falciparum* protein kinase G (PfPKG) to detect its presence in IPs with anti-PfCDPK1, anti-PfPKAr and anti-14-3-3I sera. PfPKG was not detected in IP pellets with anti-PfPKAr, ant-PfCDPK1 and anti-Pf14-3-3I sera (Fig. S4b). PfPKG was also not detected in IPs with anti-PfPKAr, ant-PfCDPK1 and anti-Pf14-3-3 sera by mass spectrometry.

The IPs described above were carried out with lysates made from merozoites resuspended in RPMI 1640, which has low K^+ levels. Next, we investigated if the interactions of Pf14-3-3I, PfPKAr and PfCDPK1 are dependent on the external ionic environment and if intracellular Ca^{2+} plays a role in these interactions. Lysates of merozoites resuspended in IC, EC and EC-BA buffers were used for IP with specific sera against PfCDPK1, PfPKAr and Pf14-3-3I. The IP elutes were probed for the presence of interacting partners. PfCDPK1 and Pf14-3-3I were detected in IPs generated with specific anti-PfPKAr sera with lysates prepared from merozoites in EC buffer (Fig. 3a). In contrast, the amounts of PfCDPK1 and Pf14-3-3I in IP elutes with anti-PfPKAr sera were significantly lower in lysates prepared from merozoites in IC and EC-BA buffers. The interactions of PfPKAr with PfCDPK1 and Pf14-3-3I are thus favored when merozoites are exposed to a low K^+ environment (Fig. 3a). Moreover, the reduced signal in IPs in case of merozoites in EC-BA buffer indicates that this interaction requires Ca^{2+}. However, the interaction between Pf14-3-3I and PfCDPK1 is not dependent on presence of Ca^{2+} (Fig. 3b and 3c). Collectively, these observations suggest that PfPKAr, PfCDPK1, and Pf14-3-3I form a multi-protein complex when merozoites are exposed to a low K^+ environment typical of blood plasma.

The interaction of PfPKAr with the multi-protein complex is dependent on the presence of intracellular Ca^{2+}, whereas the interaction of PfCDPK1 is independent of Ca^{2+}.

Size exclusion chromatography was also used to detect the presence of the multi-protein complex including PfPKAr, PfCDPK1 and Pf14-3-3I in merozoite lysates. When lysates were prepared from merozoites treated with IC buffer, PfPKAr, PfCDPK1 and Pf14-3-3I primarily migrated at positions reflecting their monomeric or dimeric sizes (Fig. 4). Some Pf14-3-3 and PfPKAr proteins were found in the higher molecular weight fractions in IC buffer, as 14-3-3 can exist in the form of homodimer (14) and PfPKAr interacts with PfPKAc (3). In contrast, when lysates were prepared from merozoites in EC buffer, PfPKAr, PfCDPK1 and Pf14-3-3I were primarily present in a high-molecular-weight complex migrating between 150 to 250 kDa (Fig. 4). Assembly of the PfPKAr, PfCDPK1, and Pf14-3-3I complex in merozoites is thus dynamic in nature and assembles in merozoites exposed to a low K^+ ionic environment (Fig. 4).

Recombinant Pf14-3-3I binds specifically to a phosphopeptide based on PfPKAr. Phosphorylation of PfPKAr at Ser 113 and Ser 114 following exposure of merozoites to EC buffer is dynamic and depends on intracellular Ca^{2+} levels (Fig. 2). The phosphorylation of PfPKAr and the interaction between PfPKAr and Pf14-3-3I are both dependent on the presence of Ca^{2+} (Figs. 2 and 3). As 14-3-3 family proteins are phospho-recognition scaffold proteins that participate in the formation of multi-protein complexes (9, 14), we hypothesized that interaction between Pf14-3-3I and PfPKAr requires Ca^{2+}-dependent phosphorylation of PfPKAr at Ser 113 and Ser 114. To test this hypothesis, we synthesized three peptides including phosphopeptide P1 spanning the sequence of phosphorylated Ser 113 and Ser 114 (NDDG**p**S**p**SDG; P1), a non-phosphorylated peptide (NDDGSSDG; P2) and a scrambled phosphorylated P1 peptide with a random distribution of the phospho-Ser residues (pSDNGpSGDD; P3). These peptides were immobilized on agarose beads and incubated with recombinant GST-tagged Pf14-3-3I protein. There was significant binding of Pf14-3-3I-GST to beads

coated with synthetic peptide P1, but none or only marginal binding to beads coated with synthetic peptides P2 and P3 (Fig. 5a). Known 14-3-3 binding peptides AA (ARSHpSYPA) and RA (RLYHpSLPA) based on canonical 14-3-3 binding motifs (15) also showed binding to Pf14-3-3I-GST similar to peptide P1 in control experiments (Fig. 5a).

Phosphopeptide from PfPKAr specifically inhibits interaction between Pf14-3-3I and PfPKAr in merozoites. Given that phosphopeptide P1 can bind to Pf14-3-3I *in vitro*, we next tested if P1 can inhibit binding of Pf14-3-3I to PfPKAr to inhibit multi-protein complex formation in merozoites. We first confirmed that peptide P1 can enter *P. falciparum* merozoites. Peptide P1 tagged with fluorophore fluorescein isothiocynate (FITC) was incubated with merozoites and tested for uptake by detecting the internalized peptide by fluorimetry (Fig. S5). Uptake of P1-FITC was observed at concentrations above 25 µM (Fig. S5). Merozoites were incubated with peptides P1, P2 and P3 at 100 µM. Subsequently, merozoite lysates were used for IP with anti-Pf14-3-3I antisera. PfPKAr and PfCDPK1 were detected in the IPs by western blotting. Phosphorylated peptide P1 inhibited the interaction between Pf14-3-3I and PfPKAr, while peptides P2 and P3 had no effect (Fig 5b). Interestingly, none of the peptides (P1, P2, and P3) had any effect on the interaction between Pf14-3-3I and PfCDPK1. The small-molecule inhibitor BV02 that blocks binding of mammalian 14-3-3 to its phosphorylated target proteins (15,16), inhibited binding of both PfPKAr and PfCDPK1 with Pf14-3-3I (Fig. 5c).

Blocking Pf14-3-3I interactions inhibits merozoite invasion of RBCs and microneme secretion. We observed above that a low K^+ environment triggered Pf14-3-3I mediated formation of a high-molecular-weight multi-protein complex composed of PfCDPK1, PfPKAr, and PKAc, all of which are involved in RBC invasion (4, 5, 17). Next, we investigated if disruption of Pf14-3-3I-mediated binding

of PfPKAr and PfCDPK1 can inhibit RBC invasion. *P. falciparum* merozoites isolated in low K^+ buffer were treated with increasing concentrations of peptides P1, P2 and P3 (10 μM, 50 μM or 100 μM) and BV02 (0.5 μM, 1 μM, 1.5 μM or 2 μM). Treated merozoites were then incubated with RBCs in complete RPMI medium to allow invasion. Newly invaded ring-stage parasites were scored by flow cytometry. Treatment of merozoites with peptide P1 and BV02 reduced the efficiency of erythrocyte invasion in a dose-dependent manner (Fig. 6a). Control peptides, P2 (without phosphorylation) and P3 (scrambled phosphopeptide) had no inhibitory effect on invasion.

The secretion of parasite invasion ligands from micronemes is a critical step in the invasion process (2). Given that PfCDPK1 and PfPKAr have both been implicated in microneme secretion (4, 5), we examined if disruption of the high-molecular-weight multi-protein complex composed of PfCDPK1, PfPKAr, and PKAc, can disrupt microneme secretion. Treatment of merozoites with peptide P1 inhibited secretion of microneme protein PfAMA1, whereas control peptides P2 and P3 had no effect (Fig. 6b). BV02 and peptides AA and RA also inhibit PfAMA1 discharge (Fig. 6b). Formation of the Pf14-3-3I-mediated multi-protein complex, which includes PfCDPK1 and PfPKAr, thus appears to be important for regulation of microneme secretion, a key step in the invasion process.

Discussion

Though there are many studies describing the intraerythrocytic phosphoproteomic profiles of *P. falciparum* blood stages, only one previous study described the phosphoproteome of free merozoites (12). However, it did not address dynamic changes in the merozoite phosphoproteome during the key process of RBC invasion. Here, we have investigated changes in the phosphoproteome of free merozoites following exposure to the environmental signal of low K^+ as found in blood plasma during the process of invasion following egress from schizonts.

The study identified signal-dependent changes in phosphorylation of merozoite proteins shedding light on molecular events that govern RBC invasion. Gene Ontology and protein-protein interaction analyses predicted that a significant number of the phosphorylated proteins identified in merozoites have potential roles in signaling and invasion related processes. Analysis of protein interaction data indicated that various proteins from these categories cluster together (Fig. 1b). Of these, the most notable invasion related proteins are inner membrane complex (IMC) proteins like PfIMC1c and PfIMC1g that are associated with merozoite motility (1). These proteins connect to myosin filaments that form the conserved molecular machinery for merozoite motility that is necessary for invasion. Various myosin molecules, PfMyoA, PfMyoB and PfMyoE, as well as glideosome-associated proteins, PfGAP40 and PfGAP45, were phosphorylated. It has been proposed recently that regulated phosphorylation of S19 in PfMyoA may enhance force generation during parasite invasion (18).

At the time of merozoite egress and re-invasion, signaling cascades are initiated through the generation of second messengers including Ca^{2+}, cAMP, and cGMP (2, 3). We found that various kinases and phosphatases in MCODE cluster 1, which are regulated by these secondary messengers and are associated with the process of secretion and invasion, are phosphorylated (Fig 1b). For example, calcium-dependent protein kinase PfCDPK1, PfPKAc, PfPKAr, PfPKG and the calcium dependent phosphatase, PfCNA (3,11,12,17,19,20), were phosphorylated. Our previous studies have demonstrated

that exposure of merozoites to a low K^+ environment in blood plasma following egress results in a rise in cytosolic Ca^{2+}, which initiates the release of invasion-related microneme proteins (5). We investigated changes in protein phosphorylation following the transfer of free merozoites from a buffer with high K^+ (IC buffer) to one with low K^+ (EC buffer). The role of intracellular Ca^{2+} in phosphorylation was also investigated by transferring merozoites to EC buffer with the intracellular Ca^{2+} chelator, BAPTA-AM (EC-BA). Phosphorylation changes occurred at 394 sites located on 314 peptides, with 76 peptides having dual phosphorylations when merozoites were transferred from IC to EC buffer. Out of these 143 phosphorylation events were found to be Ca^{2+}-dependent and were located on 119 peptides, 24 of which displayed dual phosphorylations. The employment of IMAC-based enrichment identified many dual phosphorylation events, which were not previously reported. Such dual phosphorylations can influence the activity of kinases. For example, dual phosphorylation of extracellular signal-regulated kinase 2 (ERK2) increases its activity by 10- to 100-fold (21). We observed many calcium-dependent dual phosphorylations on proteins with diverse functions in the life cycle of the parasite. These included proteins known to be involved in organelle secretion and invasion-related processes. For example, dual phosphorylation of inner membrane complex (IMC) protein, PfIMC1g, at Thr189/Ser191 and Tyr272/Ser274, and the glideosome−associated protein 45 (PfGAP45) at Ser156/Thr158 was observed. Both these proteins are known to be phosphorylated by a calcium-dependent kinase, PfCDPK1 (17). We also observed Ca^{2+}-dependent dual phosphorylation of PfPKAr at Ser113/Ser114, but by contrast dual phosphorylation at Ser28/Ser34 of PfCDPK1 was not Ca^{2+}-dependent.

Interactions between PfPKAr and PfCDPK1 and between PfPKAr and Pf14-3-3I have been observed previously (17,22). Here, we demonstrated that these interactions are phosphorylation-dependent and dynamic (Fig. 3). Moreover, they lead to the formation of a high-molecular-weight (150-250 kDa) multi-protein signaling complex that assembles in response to a change in the environmental ionic composition to which egressed merozoites are exposed (Fig 4d). PfCDPK1 was

previously shown to be present in merozoites in a high-molecular-weight complex, but the composition and dynamic nature of the complex was not described (11). A related study has shown by immunofluorescence microscopy that Pf14-3-3I colocalizes with PfCDPK1 at the periphery of merozoites (23). Our mass spectrometric analyses demonstrated that the complex contains PfCDPK1, Pf14-3-3I, PfPKAr, and PfPKAc, but interestingly, it failed to detect PfPKG that has also been implicated in apical organelle secretion at the time of merozoite invasion (24). A previous study on protein signaling complexes also did not detect PfPKG in the high-molecular-weight complex with PfCDPK1 (11).

Members of the 14-3-3 family of scaffold proteins bind target proteins in a phosphorylation-dependent manner through recognition of optimal consensus sequence motifs corresponding to mode-I (RXXpS/pT), mode-II (RXXXpS/pT) or mode-III (RXXpS/pTX1-2 C'), thus regulating a wide variety of cellular processes (25-28). Disruption of the interactions mediated by 14-3-3 proteins results in ablation of key cellular processes (17). Here, we show that peptides based on the dual phosphorylation of PfPKAr at Ser 113 and Ser 114 (peptide P1), as well as inhibitory peptides, AA and RA, that are based on consensus sequences in 14-3-3 binding proteins from mammalian cells, and 14-3-3 based inhibitory small molecule, BV02, all inhibited the formation of the multi-protein complex (Fig. 5b, c). The inhibitory peptides and BV02 also blocked secretion of microneme protein PfAMA1 and RBC invasion, demonstrating that assembly of this signaling complex plays a critical role in these processes (Fig. 6). A related study has confirmed the phosphorylation dependent interaction of recombinant Pf14-3-3I and PfCDPK1 using ELISA plate based binding assays as well as surface plasmon resonance (SPR) and isothermal calorimetry (ITC) (23). Moreover, the study shows that peptides AA and RA inhibit PfCDPK1 binding with Pf14-3-3I and block blood stage parasite growth (23). Here, we demonstrate that phosphopeptides, P1 and P2, that are based on PfPKAr sequences that interact with Pf14-3-3I, inhibit interaction of PfPKAr with Pf14-3-3I and block miconeme secretion and RBC invasion by *P. falciparum* merozoites.

14-3-3 homologs in mammalian cells are known to serve as the central hub for signaling networks that regulate cell proliferation, adhesion, survival, and apoptosis (15). Given its central role in cell growth, 14-3-3 is also implicated in the development of cancer, and small molecule inhibitors that target its scaffold function are being developed for cancer therapy (29). In this study, we have shown that targeting the assembly of the multi-protein complex in merozoites mediated by Pf14-3-3I provides a novel strategy to inhibit the blood-stage growth of malaria parasites.

Materials and Methods

***P. falciparum* merozoite isolation.** *P. falciparum* 3D7 blood stages were cultured *in vitro* and merozoites were isolated as previously described (5,30). Mature synchronized schizonts were transferred to IC buffer (142 mM KCl, 5 mM NaCl, 2 mM EGTA, 1 mM $MgCl_2$, 5.6 mM glucose, 25 mM Hepes, pH 7.2). Released merozoites were collected by centrifugation as described previously (5) and resuspended in IC buffer, EC buffer (5mM KCl, 142 mM NaCl, 1 mM $CaCl_2$, 1 mM $MgCl_2$, 5.6 mM glucose and 25 mM Hepes, pH 7.2) or EC-BA buffer (EC buffer supplemented with 50 mM BAPTA-AM (Calbiochem)) at 37^0C for 15 mins with or without inhibitors as required. Merozoites pellets were prepared by centrifugation at 3300g for 5 min and stored at -80ºC for further analysis.

Protein isolation, desalting, and digestion. Isolated merozoites were lysed by incubation with urea lysis buffer on ice for 15 min followed by sonication for 3 x 30 seconds on ice. Protein concentration was quantified by Pierce™ BCA Protein Assay Kit as per the supplier's protocol. 6-7 mg of total protein was used for each biological replicate for the label-free phosphoproteomics experiment. For the quantitative experiment, 100 µg of total protein isolated from IC, EC, and EC-BA treated merozoites was used for labeling as described below. The isolated proteins were reduced, alkylated and digested with trypsin gold (Promega) with 1:200 enzyme to substrate ratio, at 37°C overnight. Tryptic digested

peptides from the label-free experiment were desalted with reverse-phase tC18 SepPak solid-phase extraction cartridge 500mg (Waters) as described previously (31).

Ion-exchange fractionation of *P. falciparum* merozoite lysates. Fractionation of desalted peptides was carried out with strong cation exchange (SCX) chromatography on a polySULFOETHYL-A column as described before (31). 12-15 fractions of 4ml were collected, lyophilized till the volume was reduced to 30% and desalted as described above.

Tandem Mass Tag (TMT) labeling and fractionation using hydrophilic interaction liquid chromatography (HILIC). Proteins isolated from merozoites in IC, EC, and EC-BA buffers were digested with trypsin and peptides were labeled separately with TMT tags with mass 128, 129 and 130 respectively as per the manufacturer's instructions. Labeled peptide samples were combined and fractionated by HILIC using method described previously (32). 12-15 fractions (0.5 ml) were collected and lyophilized for further use.

Immobilized metal affinity chromatography (IMAC) and TiO_2/ZrO_2 phosphopeptide enrichment and desalting. Combined IMAC based phosphoproteomic enrichment and desalting was carried out as described previously (31). Peptide fractions were incubated on a rotating platform with IMAC beads (PHOS-Select iron affinity gel (Sigma)) for 1hr at RT. During this time StageTips (33) were prepared using Empore 3M C18 material (Fisher Scientific). After incubation, IMAC beads were added on top of the StageTips and the flow-through was collected and concentrated on a speedvac. Phosphopeptides were eluted from IMAC resin onto C18 loaded tips and desalted. Phosphopeptides were eluted from C18 StageTips, lyophilized and stored at -80°C. Flow through from IMAC was used further for

phosphopeptide enrichment using TiO_2/ZrO_2 NuTip (Glygen) as per manufacturer's protocol. Phosphopeptides were eluted, concentrated by speedvac centrifugation and stored at -20°C till further analysis.

Liquid chromatography-tandem mass spectrometry. LC-MS/MS was carried out using a Nano LC-1000 HPLC nanoflow system (Thermofisher Scientific) and hybrid Orbitrap Velos Pro mass spectrometer (Thermofisher Scientific). Peptides were separated by a 120 min gradient using Acclaim® PepMap100 C18 column and eluted onto the mass spectrometer. Data acquisition was performed in a data-dependent mode to automatically switch between MS, MS_2. Full-scan MS spectra of intact peptides (m/z 350–1000) were acquired in the Orbitrap with a resolution of 60,000. Top 20 precursors were sequentially isolated and fragmented in the high-energy collisional dissociation (HCD) cell. Dynamic exclusion was 50 s and a minimum 500 counts for Mz and 200 counts for TMT sets were required for MS_2 selection.

Data analysis for TMT and label free phosphoproteomic data. All raw files were searched against a *P. falciparum* database using an OpenMS pipeline (34) containing the two search engines Mascot and MSGF+, followed by Percolator post-processing and phosphorylation analysis using PhosphoScoring, an implementation of the Ascore algorithm (35). Search parameters were: carbamidomethylation of cysteines was set as a fixed modification, oxidation of methionine, protein N-terminal acetylation, and STY phosphorylation were set as variable modifications. The mass tolerances in MS and MS/MS were set to 20 ppm and 0.5 Da respectively. A false discovery rate of 1% was set up for both protein and peptide levels. TMT experiment, TMT-6plex labeling on lysine and N-termini was searched for protein quantitation. Phosphoscore more than 11 was considered as a significant localization score.

Data was also searched using MaxQuant (version 1.5.3.8) (with the Andromeda search engine) against a *P. falciparum* database. The following search parameters were applied: carbamidomethylation of cysteines was set as a fixed modification, oxidation of methionine, protein N-terminal acetylation, and STY phosphorylation was set as variable modifications. The mass tolerances in MS and MS/MS were set to 5 ppm and 0.5 Da respectively. A false discovery rate of 1% was set up for both protein and peptide levels. TMT-6plex labeling on Lysine and N-termini was searched for protein quantitation. Phospho-localization probability of more than 75% was considered as significant localization. Quantification from MaxQuant analysis was used for quantification of changes in the phosphorylation. All phospho-spectra of interest were manually validated.

To determine whether the variation of the quantification of a phosphopeptide is due to a variation in the abundance of the protein itself, or due to a variation in the abundance of its modification, a statistical test was performed to compare the variation in abundance of each phosphopeptide to the abundance of the corresponding protein. To do this for a specific phosphopeptide, we first estimated the average m and standard deviation s of the $\log_2$ fold change ($\log_2$FC) of the non-modified peptides of the protein (where FC is equal to either $\overline{EC}/\overline{IC}$ or $\overline{EC-BA}/\overline{IC}$, $\bar{x}$ being the average intensity observed for a peptide in the condition x). Assuming that the $\log_2$FC of the non-modified peptides follows a Normal distribution centered on m and having a standard deviation of s, we deduce a p-value related to the test that the measured $\log_2$FC for the phosphopeptide is equal to m by $2 \times P_{N(m,s)}(\log2(\mathrm{FC}))$ if $\log2(\mathrm{FC}) < \mathrm{m}$ and $2 \times (1 - P_{N(m,s)}(\log2(\mathrm{FC})))$ if $\log2(\mathrm{FC}) \geq \mathrm{m}$, where $P_{N(m,s)}$ is the cumulative distribution function of $N(m,s)$. Note that this p-value is computed only when we have at least 3 non-modified peptides with intensity values for a protein.

Phosphorylated protein interaction network analysis. The merozoite phosphoproteome interaction network was constructed using STRING database and visualized in Cytoscape version 3.7.1 (36). The merozoite phospho-interactome was analyzed for highly connected nodes with the molecular complex detection clustering algorithm MCODE (37).

Gene ontology and motif analysis. All *P. falciparum* gene ontology analyses were performed with the inbuilt result analysis tool for gene ontology on PlasmoDB database. Phosphopeptides with a width of 15 amino acids were subjected to motif analysis using MotifX (38,39). A background of *P. falciparum* protein database was used for the analysis and occurrences threshold was set to default P-value threshold of $\leq 1e^{-6}$ was used to identify enriched motifs.

Immunoprecipitation (IP), LC-MS/MS and data analysis. IP of proteins from merozoites isolated in cRPMI or resuspended in IC, EC, and EC-BA buffers or treated with specific inhibitors or peptides were performed with Pierce Co-Immunoprecipitation (Co-Ip) Kit (Pierce) as per the manufacturer's protocol. Identity of proteins from the respective elute of IP experiments was investigated using an Orbitrap Q Exactive Plus mass spectrometer (Thermofisher Scientific) or by western blotting. Data were searched using MaxQuant as described above.

Gel-filtration on Superdex 200. *P. falciparum* merozoites treated with IC or EC buffer were lysed and cleared by centrifugation. Proteins were fractionated with Superdex 200 column (GE Healthcare, 10×300 mm). Fractions of 1 ml were collected and analyzed by western blotting for the presence of PfPKAr, Pf14-3-3I, and PfCDPK1 in respective fractions.

Binding of recombinant Pf14-3-3I to synthetic peptide-coated beads. Peptides (AA, RA, P1, P2, and P3) were coupled to agarose beads using Co-IP kit (Pierce) as per manufacturer's instruction. Respective peptide coated beads were incubated with GST tagged Pf14-3-3I protein, non-coated beads were used as a control. Recombinant protein bound to the beads were eluted and elutes were tested by western blotting using anti-Pf14-3-3I mouse sera.

Invasion assay *with P. falciparum* merozoites and flow cytometry. Merozoites isolated as described above were treated with inhibitors (BV02 at 0.5µM, 1µM, 1.5µM, 2µM) and peptides (P1, P2, P3 at 10µM, 50µM, 100µM) for 15 min at 37ºC followed by incubation with RBC in presence of the inhibitor or peptide to allow invasion and growth for 24 h under standard culturing conditions. Solvents used to dissolve the inhibitors were used as control. The parasitemia was determined by flow cytometry after staining with SYBR-GreenI (Sigma) as described (40). Data were analyzed with FlowJo (Tree Star) and percent inhibition of invasion was calculated using the formula: (1- T/C) x 100; where T and C denote parasitemia in treatment and control samples respectively.

Microneme secretion assay. *P. falciparum* merozoites isolated in cRPMI were incubated for 15 min at 37°C with BV02 (2µM) or AA (100µM) or RA (100µM) or DMSO (solvent) and with Peptides P1, P2, P3 (100µM each) or RPMI (solvent). Following incubation, merozoites and supernatants were separated by centrifugation and the presence of PfAMA1 (microneme protein), and PfNapL (cytosolic protein used as lysis control) in the supernatant, and PfNapL in the pellet (cytosolic protein used as a loading control) were detected by western blotting as described above.

Densitometry and statistical analysis. Image J (NIH) software was used to perform densitometry of western blots. The band intensity of the loading control was used for normalization. Statistical analysis for all the plots was performed using GraphPad Prism 8.1.2 software. All experiments were analyzed using multiple *t*-test (assuming equal standard error (SE)) and $P \leq 0.05$ was considered significant, *= $P < 0.05$; **= $P < 0.005$; and ***= $P < 0.0005$. The graphs were plotted with a mean ± SEM of the population.

Data availability. The mass spectrometry-based proteomics data have been deposited to the ProteomeXchange Consortium (http://proteomecentral.proteomexchange.org) via the PRIDE (41) partner repository with the data set identifier PXD015093.

Reviewer account details: Username: reviewer83422@ebi.ac.uk; Password: MNKnPy0v

All other relevant data are available from the authors upon request.

Acknowledgments

This work was supported by MolSigMal grant (ANR-17-CE15-0010) from Agence Nationale de la Recherche (ANR) to CEC and internal funds from the Institut Pasteur. GL acknowledges support from the Labex ParaFrap (ANR-11-LABX-0024). KRM received a Short Term Fellowship from European Molecular Biology Organization (EMBO).

Author Contributions

KRM designed and performed all experiments, analyzed data and wrote the first draft of the manuscript; IK performed MS/MS experiments and preliminary analysis; QGG and BI performed bio-informatic and statistical analysis of phosphoproteomics data; TC performed MS/MS analysis of immunoprecipitation experiments; RJ produced reagents (antibodies to Pf14-3-3 and plasmid construct for expression of recombinant Pf14-3-3I); CH produced recombinant Pf14-3-3 for use in binding experiments and performed GPC to detect multi-protein complexes in parasite lysates; MM supervised MS/MS experiments and data analysis; HW and PG helped with analysis of phosphoproteomics data; JC supervised MS/MS data analysis; GL provided reagents (antibodies against PfPKAr and PfPKAc), helped design experiments and analyze data and edited the manuscript; SS contributed reagents (antibodies to Pf14-3-3I, plasmid construct for production of recombinant Pf14-3-3I), helped design experiments and analyzed data; CC created the project, raised funds, designed experiments, analyzed data and edited the manuscript. All authors reviewed and commented on the manuscript.

References

1. Gaur D, Chitnis CE. 2011. Molecular interactions and signaling mechanisms during erythrocyte invasion by malaria parasites. Curr Opin Microbiol 14:422-8.
2. Sharma P, Chitnis CE. 2013. Key molecular events during host cell invasion by Apicomplexan pathogens. Curr Opin Microbiol 16:432-7.
3. Baker DA, Drought LG, Flueck C, Nofal SD, Patel A, Penzo M, Walker EM. 2017. Cyclic nucleotide signalling in malaria parasites. Open Biol 7(12).doi:10.1098/rsob.1-70213.
4. Dawn A, Singh S, More KR, Siddiqui FA, Pachikara N, Ramdani G, Langsley G, Chitnis CE. 2014. The central role of cAMP in regulating Plasmodium falciparum merozoite invasion of human erythrocytes. PLoS Pathog 10:e1004520.
5. Singh S, Alam MM, Pal-Bhowmick I, Brzostowski JA, Chitnis CE. 2010. Distinct external signals trigger sequential release of apical organelles during erythrocyte invasion by malaria parasites. PLoS Pathog 6:e1000746.
6. Day EK, Sosale NG, Lazzara MJ. 2016. Cell signaling regulation by protein phosphorylation: a multivariate, heterogeneous, and context-dependent process. Curr Opin Biotechnol 40:185-192.
7. Ardito F, Giuliani M, Perrone D, Troiano G, Lo Muzio L. 2017. The crucial role of protein phosphorylation in cell signaling and its use as targeted therapy (Review). Int J Mol Med 40:271-280.
8. Blonska M, Lin X. 2011. NF-kappaB signaling pathways regulated by CARMA family of scaffold proteins. Cell Res 21:55-70.
9. Agarwal-Mawal A, Qureshi HY, Cafferty PW, Yuan Z, Han D, Lin R, Paudel HK. 2003. 14-3-3 connects glycogen synthase kinase-3 beta to tau within a brain microtubule-associated tau phosphorylation complex. J Biol Chem 278:12722-8.
10. Kawamoto N, Sasabe M, Endo M, Machida Y, Araki T. 2015. Calcium-dependent protein kinases responsible for the phosphorylation of a bZIP transcription factor FD crucial for the florigen complex formation. Sci Rep 5:8341.
11. Alam MM, Solyakov L, Bottrill AR, Flueck C, Siddiqui FA, Singh S, Mistry S, Viskaduraki M, Lee K, Hopp CS, Chitnis CE, Doerig C, Moon RW, Green JL, Holder AA, Baker DA, Tobin AB. 2015. Phosphoproteomics reveals malaria parasite Protein Kinase G as a signalling hub regulating egress and invasion. Nat Commun 6:7285.
12. Lasonder E, Green JL, Grainger M, Langsley G, Holder AA. 2015. Extensive differential protein phosphorylation as intraerythrocytic Plasmodium falciparum schizonts develop into extracellular invasive merozoites. Proteomics 15:2716-29.
13. Bansal A, Singh S, More KR, Hans D, Nangalia K, Yogavel M, Sharma A, Chitnis CE. 2013. Characterization of Plasmodium falciparum calcium-dependent protein kinase 1 (PfCDPK1) and its role in microneme secretion during erythrocyte invasion. J Biol Chem 288:1590-602.
14. Morrison DK. 2009. The 14-3-3 proteins: integrators of diverse signaling cues that impact cell fate and cancer development. Trends Cell Biol 19:16-23.
15. Mancini M, Corradi V, Petta S, Barbieri E, Manetti F, Botta M, Santucci MA. 2011. A new nonpeptidic inhibitor of 14-3-3 induces apoptotic cell death in chronic myeloid leukemia sensitive or resistant to imatinib. J Pharmacol Exp Ther 336:596-604
16. Ottmann C. 2013. Small-molecule modulators of 14-3-3 protein-protein interactions. Bioorg Med Chem 21:4058-62.

17. Kumar S, Kumar M, Ekka R, Dvorin JD, Paul AS, Madugundu AK, Gilberger T, Gowda H, Duraisingh MT, Keshava Prasad TS, Sharma P. 2017. PfCDPK1 mediated signaling in erythrocytic stages of Plasmodium falciparum. Nat Commun 8:63.
18. Robert-Paganin J, Robblee JP, Auguin D, Blake TCA, Bookwalter CS, Krementsova EB, Moussaoui D, Previs MJ, Jousset G, Baum J, Trybus KM, Houdusse A. 2019. Plasmodium myosin A drives parasite invasion by an atypical force generating mechanism. Nat Commun 10:3286.
19. Lasonder E, Green JL, Camarda G, Talabani H, Holder AA, Langsley G, Alano P. 2012. The Plasmodium falciparum schizont phosphoproteome reveals extensive phosphatidylinositol and cAMP-protein kinase A signaling. J Proteome Res 11:5323-37.
20. Singh S, More KR, Chitnis CE. 2014. Role of calcineurin and actin dynamics in regulated secretion of microneme proteins in Plasmodium falciparum merozoites during erythrocyte invasion. Cell Microbiol 16:50-63.
21. Prowse CN, Lew J. 2001. Mechanism of activation of ERK2 by dual phosphorylation. J Biol Chem 276:99-103.
22. Bandje K, Naissant B, Bigey P, Lohezic M, Vayssieres M, Blaud M, Kermasson L, Lopez-Rubio JJ, Langsley G, Lavazec C, Deloron P, Merckx A. 2016. Characterization of an A-kinase anchoring protein-like suggests an alternative way of PKA anchoring in Plasmodium falciparum. Malar J 15:248.
23. Jain R, Dey P, Gupta S, Pati S, Bhattacharjee A, Munde M, Singh S. 2020. Interaction of 14-3-3I and CDPK1 mediates the growth of human malaria parasites. bioRxiv. doi:https://doi.org/10.1101/2020.01.14.906479
24. Collins CR, Hackett F, Strath M, Penzo M, Withers-Martinez C, Baker DA, Blackman MJ. 2013. Malaria parasite cGMP-dependent protein kinase regulates blood stage merozoite secretory organelle discharge and egress. PLoS Pathog 9:e1003344.
25. Muslin AJ, Tanner JW, Allen PM, & Shaw AS. 1996. Interaction of 14-3-3 with signaling proteins is mediated by the recognition of phosphoserine. Cell, 84(6), 889-897.
26. Yaffe MB, Rittinger K, Volinia S, Caron PR, Aitken A, Leffers H, Pascarela S, Rinaldo S, Visconti S, Cantley LC. 1997. The structural basis for 14-3-3:phosphopeptide binding specificity. Cell, 91(7), 961-971.
27. Coblitz B, Wu M, Shikano S, & Li M. 2006. C-terminal binding: an expanded repertoire and function of 14-3-3 proteins. FEBS Lett, 580(6), 1531-1535.
28. Paiardini A, Aducci P, Cervoni L, Cutruzzola F, Di Lucente C, Janson G, . . . Camoni L. 2014. The phytotoxin fusicoccin differently regulates 14-3-3 proteins association to mode III targets. IUBMB Life, 66(1), 52-62.
29. Matta A, Siu KW, Ralhan R. 2012. 14-3-3 zeta as novel molecular target for cancer therapy. Expert Opin Ther Targets 16:515-23.
30. Trager W, & Jensen JB. 1976. Human malaria parasites in continuous culture. Science, 193(4254), 673-675.
31. Villen J, Gygi SP. 2008. The SCX/IMAC enrichment approach for global phosphorylation analysis by mass spectrometry. Nat Protoc 3:1630-8.
32. Solyakov L, Halbert J, Alam MM, Semblat JP, Dorin-Semblat D, Reininger L, Bottrill AR, Mistry S, Abdi A, Fennell C, Holland Z, Demarta C, Bouza Y, Sicard A, Nivez MP, Eschenlauer S, Lama T, Thomas DC, Sharma P, Agarwal S, Kern S, Pradel G, Graciotti M,

Tobin AB, Doerig C. 2011. Global kinomic and phospho-proteomic analyses of the human malaria parasite Plasmodium falciparum. Nat Commun 2:565.

33. Rappsilber J, Mann M, & Ishihama Y. 2007. Protocol for micro-purification, enrichment, pre-fractionation and storage of peptides for proteomics using StageTips. Nat Protoc, 2(8), 1896-1906.
34. Weisser H, Wright JC, Mudge JM, Gutenbrunner P, & Choudhary JS. 2016. Flexible Data Analysis Pipeline for High-Confidence Proteogenomics. J Proteome Res, 15(12), 4686-4695.
35. Beausoleil SA, Villén J, Gerber SA, Rush J, Gygi SP. (2006) A probability-based approach for high-throughput protein phosphorylation analysis and site localization. Nat Biotechnol. Oct;24(10):1285-92.
36. Shannon P, Markiel A, Ozier O, Baliga NS, Wang JT, Ramage D, Amin N, Schwikowski B, Ideker T. 2003. Cytoscape: a software environment for integrated models of biomolecular interaction networks. Genome Res 13:2498-504.
37. Bader GD, Hogue CW. 2003. An automated method for finding molecular complexes in large protein interaction networks. BMC Bioinformatics 4:2.
38. Chou MF, Schwartz D. 2011. Biological sequence motif discovery using motif-x. Curr. Protocs. Bio-informatics. Chapter 13, Unit 13 15-24. Doi:10.1002/0471250953.b11315s35.
39. Schwartz D and Gygi SP 2005. An iterative statistical approach to the identification of protein phosphorylation motifs from large scale datasets. Nat. Biotech
40. Bei AK, Desimone TM, Badiane AS, Ahouidi AD, Dieye T, Ndiaye D, Sarr O, Ndir O, Mboup S, Duraisingh MT. 2010. A flow cytometry-based assay for measuring invasion of red blood cells by Plasmodium falciparum. Am J Hematol 85:234-7.
41. Perez-Riverol Y, Csordas A, Bai J, Bernal-Llinares M, Hewapathirana S, Kundu DJ, Inuganti A, Griss J, Mayer G, Eisenacher M, Pérez E, Uszkoreit J, Pfeuffer J, Sachsenberg T, Yilmaz S, Tiwary S, Cox J, Audain E, Walzer M, Jarnuczak AF, Ternent T, Brazma A, Vizcaíno JA. 2019. The PRIDE database and related tools and resources in 2019: improving support for quantification data. Nucleic Acids Res. 47(D1):D442-D450.

631 **Table 1. Identification of PfCDPK1, PfPKAr, Pf14-3-3I and PfPKAc by mass spectrometry.** The

632 complete list of proteins identified in the immunoprecipitates is reported in Supplementary Table S4.

Protein detected in IP		Max Quant Score	IP with anti-PfPKAr		IP with anti-PfCDPK1		IP with anti-Pf14-3-3I	
protein ID	Protein name		Unique peptides	Sequence coverage [%]	Unique peptides	Sequence coverage [%]	Unique peptides	Sequence coverage [%]
PF3D7_0217500	PfCDPK1	323.31	39	62	57	66.6	43	66.4
PF3D7_1223100	PfPKAr	323.31	36	69.2	49	74.6	34	71.4
PF3D7_0818200	Pf14-3-3I	323.31	20	67.2	19	58.4	20	74

633

634

635 **Figure Legends.**

636 **Figure 1. The phosphoproteome of *P. falciparum* merozoites: a.)** Venn diagram depicting overlap in
637 phosphorylation sites and phosphorylated proteins between the published merozoite phosphoproteome
638 (12) and this study. **b)** Signaling and invasion related proteins from clustered subnetwork 1 from
639 merozoite interaction network of phosphorylated proteins using MCODE clustering algorithm. Protein
640 interaction data were downloaded from STRING for phosphoproteins found in this study and
641 visualized in Cytoscape. MCODE clustering algorithm was used for the generation of the subnetwork
642 of highly interacting proteins and each cluster was analyzed to identify overrepresented molecular
643 function categories. Interaction network of proteins corresponding to molecular function category,
644 Invasion of host cells and signaling related proteins from MCODE cluster 1, is shown here. Invasion-
645 related proteins are in green, while signaling related proteins are in pink.

646

647 **Figure 2. Signal-dependent changes in phosphoproteome of *P. falciparum* merozoites: a)** Fold-
648 changes in abundance of phosphopeptides in merozoites in EC buffer with low K^+ compared to IC
649 buffer with high K^+ were plotted against fold-changes of non-phosphopeptides. **b)** Fold-changes in
650 phosphopeptides in merozoites in EC + BAPTA-AM (EC-BA) buffer compared to IC buffer plotted
651 against fold-changes of non-phosphopeptides. p-values for fold change in phosphorylation (colour
652 coded) were calculated, as compared to the changes in non-phosphorylated peptides for respective
653 proteins. Key proteins and their phosphosites with significant alterations are shown. **c.)** Fold-changes in
654 individual phosphorylations in EC compared with IC and EC-BA compared with IC for PfCDPK1. The
655 grey area represents fold-change in abundance of non-phosphorylated peptides from the corresponding
656 proteins. Phosphosites with significant changes in abundance lie outside the grey area and are denoted
657 with triangles. Phosphorylation of Ser 28/34 and Ser 64 of PfCDPK1 was significantly higher in EC
658 and EC-BA compared to IC. **d.)** Fold-changes in individual phosphorylations in EC compared with IC

and EC-BA compared with IC for PfPKAr. The grey area represents fold-change in abundance of non-phosphorylated peptides from the corresponding proteins. Phosphosites with significant changes in abundance lie outside the grey area and are denoted with triangles. Phosphorylation of PfPKAr on Ser113/Ser114 was significantly higher in EC buffer, but not EC-BA buffer, compared to IC buffer.

Figure 3. Calcium-dependent interaction of PfPKAr with PfCDPK1 and Pf14-3-3I leads to formation of a multi-protein complex in *P. falciparum* merozoites: a) PfPKAr was immunoprecipitated (IP) from merozoites in IC buffer mimicking intracellular ionic conditions with high K^+ (IC), EC buffer mimicking extracellular ionic conditions with low K^+, or EC buffer with intracellular Ca^{2+} chelator BAPTA-AM (EC-BA). The presence of PfCDPK1, Pf14-3-3I and PfPKAr in IPs was confirmed by western blotting. Graphs show the average intensity normalized with the protein immunoprecipitated for each condition from three independent experiments. A representative western blotting image from one of three independent experiments is shown. **b)** and **c)** show representative western blotting images for IPs with specific anti-Pf14-3-3I and anti-PfCDPK1 sera, respectively; with quantification of interaction partners from 3 independent experiments shown in bar graphs. Mean ± SEM are shown with n=3, * indicates $P < 0.05$, ** indicates $P < 0.005$, *** indicates $P < 0.0005$ by t-test. NS, non-significant, $P > 0.05$.

Figure 4. Analysis of assembly of multi-protein complexes with PfPKAr, PfCDPK1 and Pf14-3-3 by gel filtration chromatography. Lysates were prepared from merozoites in IC and EC buffers and fractionated using a Superdex 200 gel filtration column. Fractions were probed for the presence of PfCDPK1, Pf14-3-3I, and PfPKAr by western blotting. Representative blots are shown for one out of three independent experiments. Intensity for each lane (representing each fraction) was measured using

682 ImageJ software and the ratio of EC/IC was calculated. The graph represents the average of the EC/IC
683 ratio for each protein from three independent experiments. Mean ± SEM are shown for 3 independent
684 experiments (n=3). * indicates $P < 0.05$, ** indicates $P < 0.005$, *** indicates $P < 0.0005$ by t-test.

685

686 **Figure 5. Inhibition of interaction between PfPKAr and Pf14-3-3I by a PfPKAr-derived**
687 **phosphopeptide, P1, and small-molecule inhibitor, BV02, of Pf14-3-3I. a)** Binding of Pf14-3-3I
688 with phosphopeptide P1 from PfPKAr. Phosphopeptide P1 (NDDGpSpSDG) based on amino acid
689 sequence of calcium-dependent phosphosites on PfPKAr encompassing S113 and S114, non-
690 phosphorylated control peptide P2 (NDDGSSDG) and peptide P3 (pSDNGpSGDD), a control
691 phosphopeptide based on scrambled P1 sequence, were tested for binding to Pf14-3-3I. Peptides P1, P2
692 and P3 were immobilized on agarose beads and allowed to interact with recombinant Pf14-3-3I. Bound
693 recombinant Pf14-3-3I was detected in elutes by western blotting. Phosphopeptides AA and RA, which
694 are known to bind 14-3-3 were used as positive controls. Control beads with no immobilized peptides
695 were used as negative control. Plots show the average percentage binding calculated for binding of
696 recombinant Pf14-3-3I to each peptide from 3 independent experiments. A representative western
697 blotting image from one out of three independent experiments is shown. **b)** Peptide P1 inhibits binding
698 of Pf14-3-3 to PfPKAr in merozoites. Merozoites were treated with 100 μM P1, P2, P3, or RPMI.
699 Merozoites were lysed and lysates were used for immunoprecipitation with anti-Pf14-3-3I sera.
700 Presence of PfCDPK1 and PfPKAr in the immunoprecipitates was investigated by western blotting.
701 Percent inhibition of binding of PfCDPK1 and PfPKAr with Pf14-3-3I was calculated. The plot shows
702 average percent inhibition of binding for three independent experiments. P1 decreases binding of
703 PfPKAr to Pf14-3-3I, but has no effect on PfCDPK1 binding to Pf14-3-3I. **c)** BV02, a small molecule
704 inhibitor of 14-3-3 interactions with phosphopeptides, inhibits binding of Pf14-3-3I to PfCDPK1 and
705 PfPKAr in merozoites. Merozoites were treated with 2 μM BV02 or DMSO and lysed, lysates were

used for immunoprecipitation with specific anti-Pf14-3-3I serum. Presence of PfCDPK1 and PfPKAr in the immunoprecipitates was confirmed by western blotting. The plot shows the mean percent inhibition of binding (± SEM) for three independent experiments (n=3). * indicates $P < 0.05$, ** indicates $P < 0.005$, *** indicates $P < 0.0005$, by t-test. NS, not significant ($P > 0.05$).

Figure 6. Inhibition of RBC invasion and microneme secretion by both PfPKAr-based phosphopeptide and Pf14-3-3I inhibitor. a) Peptide P1 and BV02 both block RBC invasion by merozoites. *P. falciparum* merozoites were isolated and allowed to invade erythrocytes in the presence of increasing concentrations of peptides P1, P2 amd P3 (10, 50 and 100 µM) and increasing concentrations of BV02 (0.5, 1, 1.5 and 2 µM). Newly invaded trophozoites were stained with SYBR green and scored by flow cytometry. Merozoites were allowed to invade erythrocytes in the absence of inhibitors using respective solvents as control. Percent invasion inhibition rates (Mean ± SEM with n=3) in presence of inhibitors are shown. ** indicates $P < 0.005$, *** indicates $P < 0.005$, t-test. **b)** Phosphopeptide P1 (NDDGpSpSDG) derived from the amino sequence of 2 calcium-dependent phosphosites on PfPKAr encompassing S113 and S114, non-phosphorylated control peptide P2 (NDDGSSDG) and peptide P3 (pSDNGpSGDD), a control phosphopeptide based on scrambled P1 sequence, AA and RA, 2 phosphopeptides based on 14-3-3 substrate binding sites, and BV02, a small molecule 14-3-3 binding inhibitor were tested for inhibition of PfAMA1 secretion by merozoites**.** Secretion of PfAMA1 was significantly reduced upon treatment of merozoites with phosphopeptides P1, AA and RA, and by BV02. Cytoplasmic protein PfNAPL was detected in the supernatant and used as a control for merozoite lysis. PfNAPL was detected in merozoite pellet and used as a control for normalization. Western blotting image for one out of three independent experiments is shown. The plot shows the average percent inhibition of binding for three independent experiments. Mean ± SEM are shown (n=3), ** indicates $P < 0.005$ by t-test.

730 **Figure 7. Model for assembly of a signaling complex during RBC invasion by *P. falciparum***
731 **merozoites.** Exposure of merozoites to a low K^+ ionic environment as found in blood plasma triggers a
732 signaling cascade resulting in the phosphorylation of PfCDPK1 and PfPKAr. The scaffold protein
733 Pf14-3-3I binds phosphorylated PfPKAr and PfCDPK1 leading to the formation of a high-molecular-
734 weight multi-protein complex composed of PfCDPK1, PfPKAr, PfPKAc and Pf14-3-3. Formation of
735 this signalling complex plays a regulatory role in secretion of microneme proteins and merozoite
736 invasion of RBCs.

737

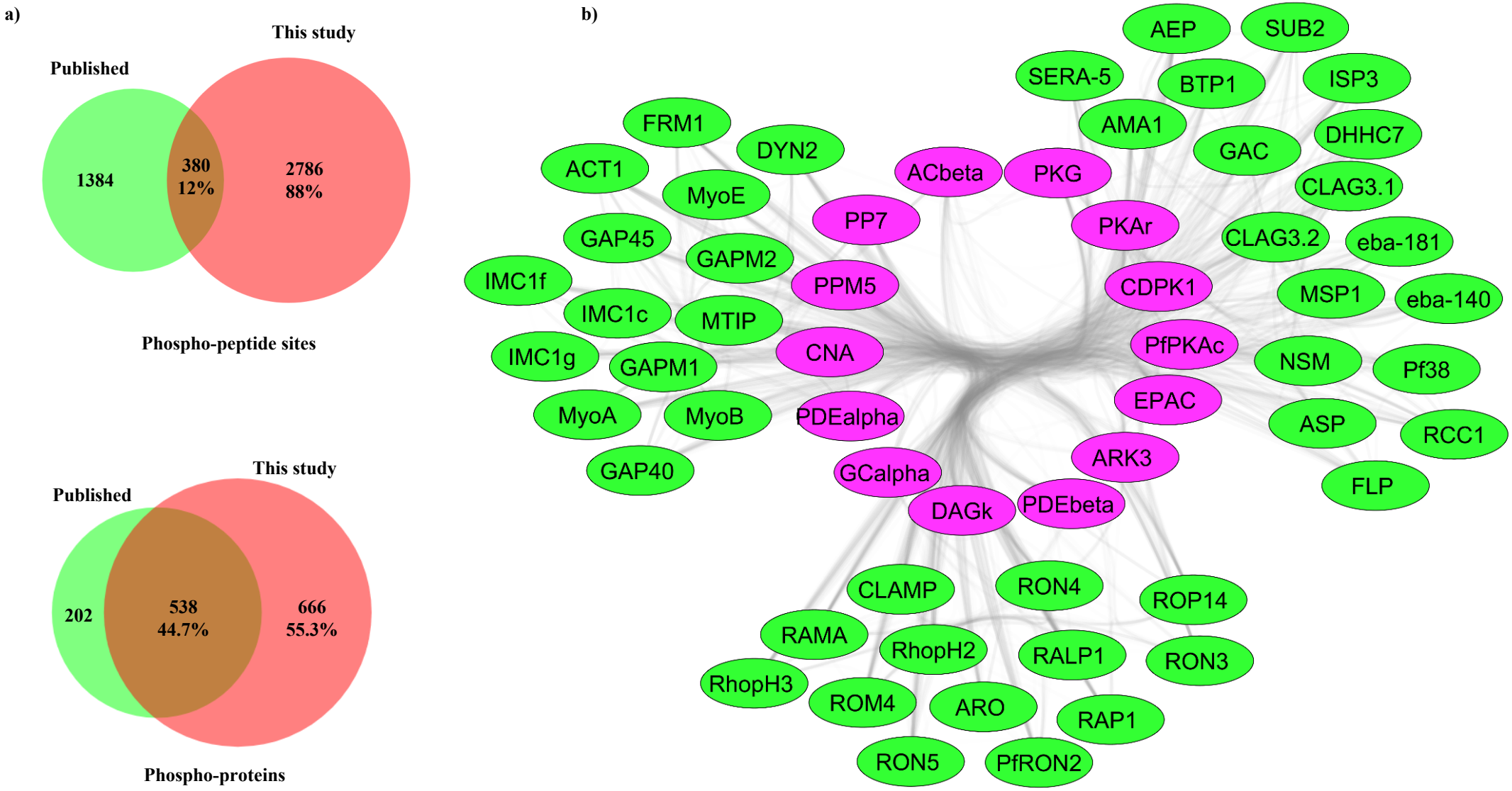
a)
This study
Published
1384
380
12%
2786
88%
Phospho-peptide sites
This study
Published
202
538
44.7%
666
55.3%
Phospho-proteins
b)
AEP
SUB2
SERA-5
BTP1
ISP3
AMA1
DHHC7
GAC
CLAG3.1
FRM1
DYN2
ACT1
ACbeta
PKG
MyoE
PP7
PKAr
CLAG3.2
eba-181
GAP45
GAPM2
IMC1f
PPM5
CDPK1
MSP1
eba-140
IMC1c
MTIP
PfPKAc
NSM
Pf38
IMC1g
GAPM1
CNA
EPAC
MyoA
MyoB
PDEalpha
ASP
RCC1
ARK3
GAP40
GCalpha
FLP
DAGk
PDEbeta
CLAMP
RON4
ROP14
RAMA
RhopH2
RALP1
RON3
RhopH3
ROM4
ARO
RAP1
RON5
PfRON2

Figure 1

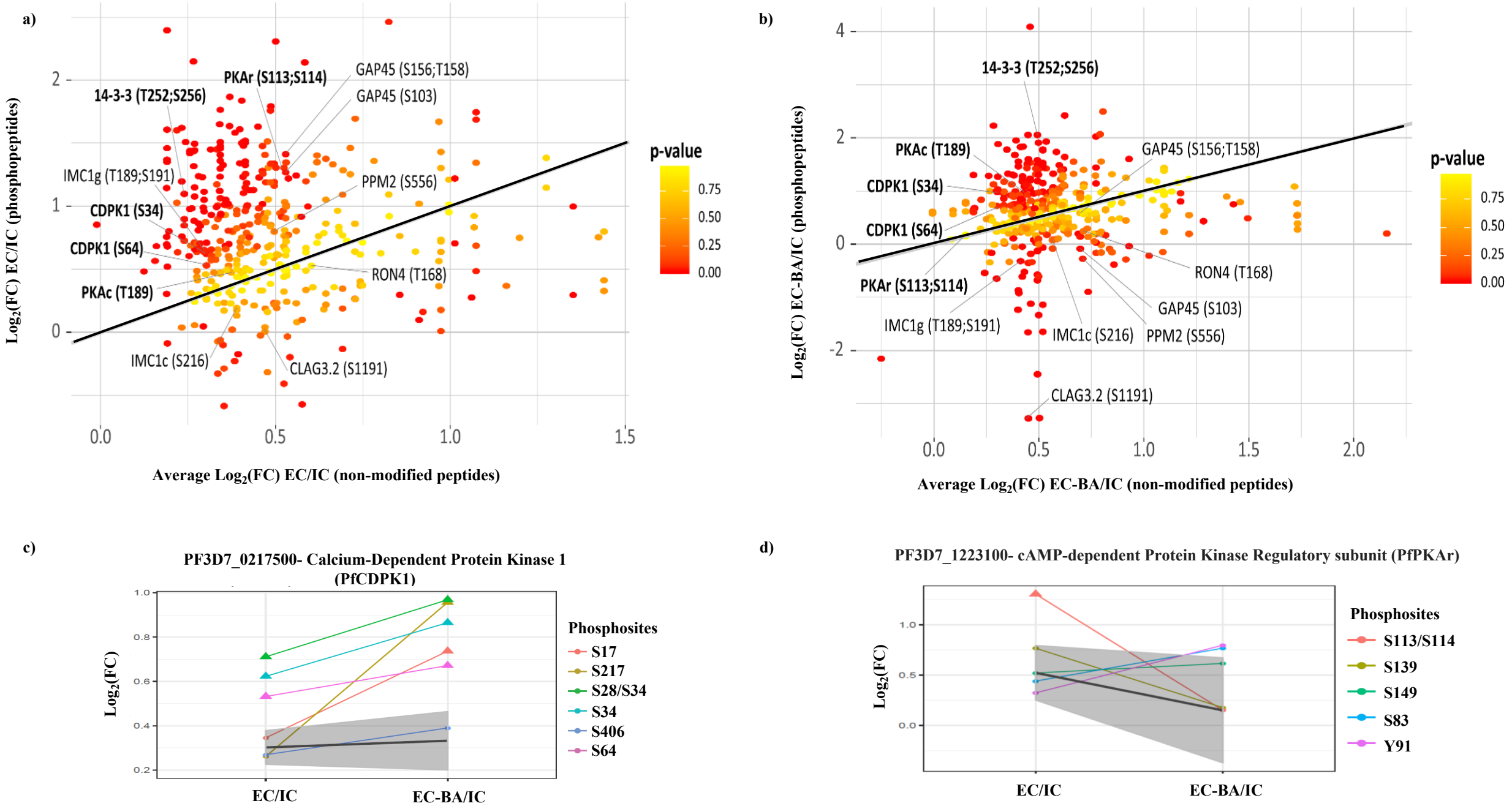
a)
Log2(FC) EC/IC (phosphopeptides)
Average Log2(FC) EC/IC (non-modified peptides)
14-3-3 (T252;S256)
PKAr (S113;S114)
GAP45 (S156;T158)
GAP45 (S103)
PPM2 (S556)
IMC1g (T189;S191)
CDPK1 (S34)
CDPK1 (S64)
RON4 (T168)
PKAc (T189)
IMC1c (S216)
CLAG3.2 (S1191)
p-value
0.75
0.50
0.25
0.00
b)
Log2(FC) EC-BA/IC (phosphopeptides)
Average Log2(FC) EC-BA/IC (non-modified peptides)
14-3-3 (T252;S256)
PKAc (T189)
GAP45 (S156;T158)
CDPK1 (S34)
CDPK1 (S64)
RON4 (T168)
PKAr (S113;S114)
GAP45 (S103)
IMC1g (T189;S191)
IMC1c (S216)
PPM2 (S556)
CLAG3.2 (S1191)
p-value
0.75
0.50
0.25
0.00
c)
PF3D7_0217500- Calcium-Dependent Protein Kinase 1 (PfCDPK1)
Log2(FC)
EC/IC
EC-BA/IC
Phosphosites
S17
S217
S28/S34
S34
S406
S64
d)
PF3D7_1223100- cAMP-dependent Protein Kinase Regulatory subunit (PfPKAr)
Log2(FC)
EC/IC
EC-BA/IC
Phosphosites
S113/S114
S139
S149
S83
Y91

Figure 2

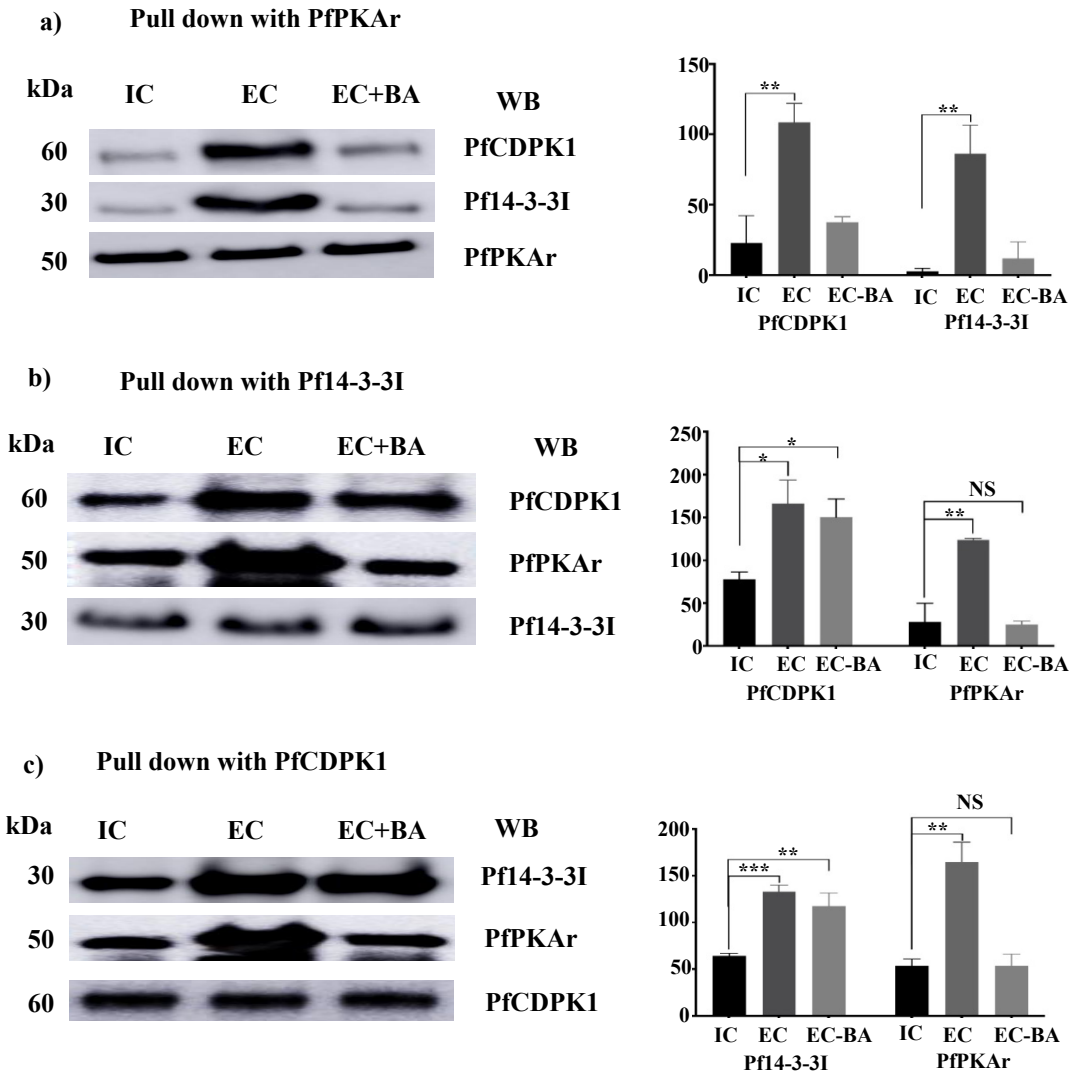
a)
Pull down with PfPKAr
kDa
IC
EC
EC+BA
WB
60
PfCDPK1
30
Pf14-3-3I
50
PfPKAr
150
100
50
0
**
**
IC EC EC-BA IC EC EC-BA
PfCDPK1
Pf14-3-3I
b)
Pull down with Pf14-3-3I
kDa
IC
EC
EC+BA
WB
60
PfCDPK1
50
PfPKAr
30
Pf14-3-3I
250
200
150
100
50
0
*
*
NS
**
IC EC EC-BA IC EC EC-BA
PfCDPK1
PfPKAr
c)
Pull down with PfCDPK1
kDa
IC
EC
EC+BA
WB
30
Pf14-3-3I
50
PfPKAr
60
PfCDPK1
200
150
100
50
0
***
**
NS
**
IC EC EC-BA IC EC EC-BA
Pf14-3-3I
PfPKAr

Figure 3

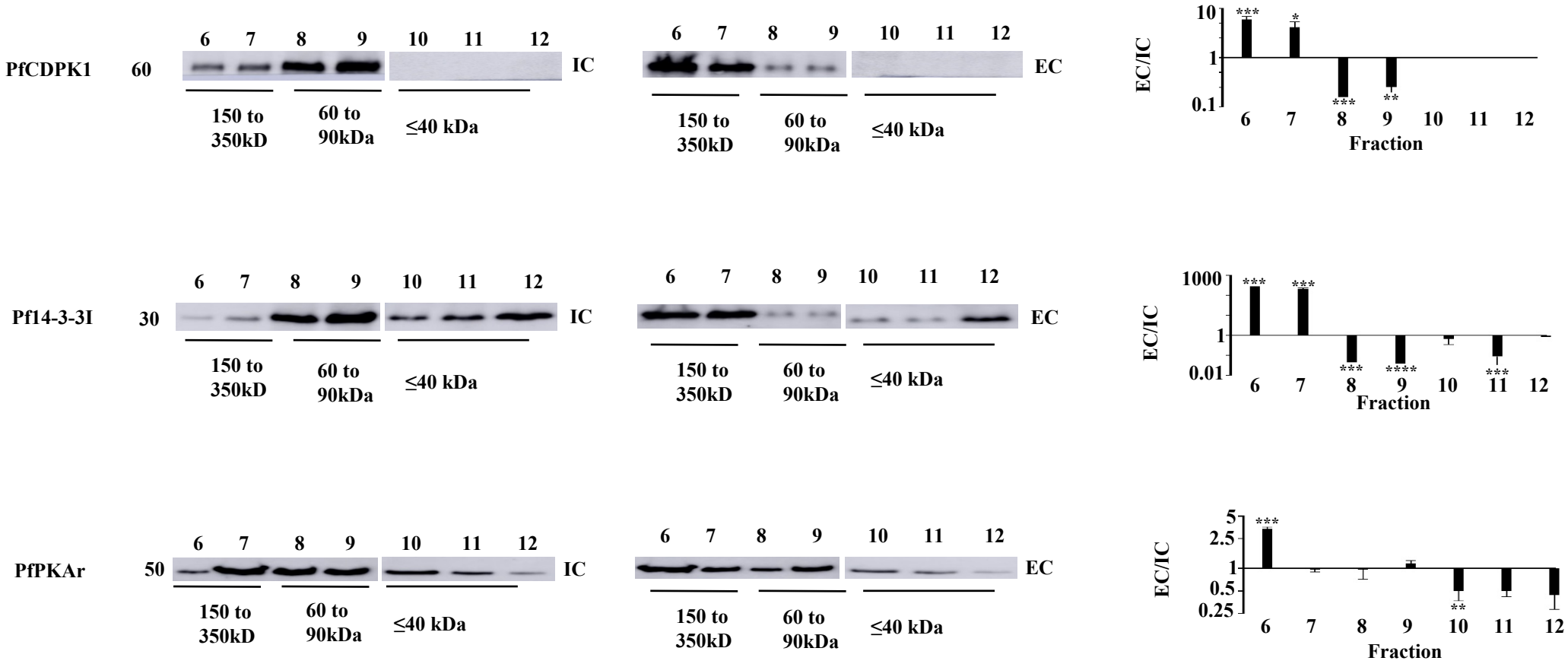
PfCDPK1
60
6 7 8 9 10 11 12
IC
150 to 350kD
60 to 90kDa
≤40 kDa
6 7 8 9 10 11 12
EC
150 to 350kD
60 to 90kDa
≤40 kDa
EC/IC
10
1
0.1
***
*
***
**
6 7 8 9 10 11 12
Fraction
Pf14-3-3I
30
6 7 8 9 10 11 12
IC
150 to 350kD
60 to 90kDa
≤40 kDa
6 7 8 9 10 11 12
EC
150 to 350kD
60 to 90kDa
≤40 kDa
EC/IC
1000
1
0.01
***
***
***
****
***
6 7 8 9 10 11 12
Fraction
PfPKAr
50
6 7 8 9 10 11 12
IC
150 to 350kD
60 to 90kDa
≤40 kDa
6 7 8 9 10 11 12
EC
150 to 350kD
60 to 90kDa
≤40 kDa
EC/IC
5
2.5
1
0.5
0.25
***
**
6 7 8 9 10 11 12
Fraction

Figure 4

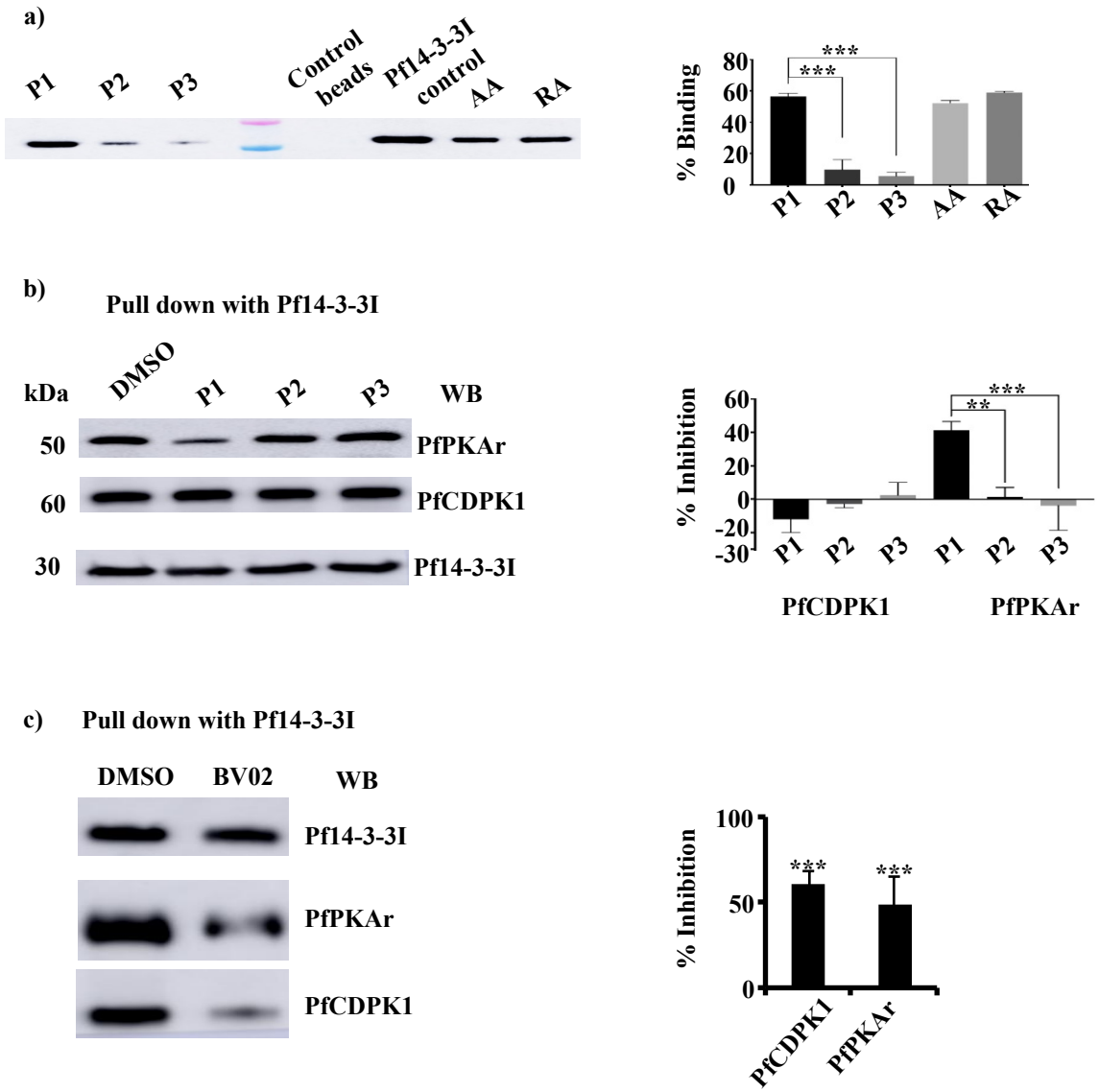
a)
P1
P2
P3
Control beads
Pf14-3-3I control
AA
RA
% Binding
***
***
80
60
40
20
0
P1
P2
P3
AA
RA
b)
Pull down with Pf14-3-3I
kDa
DMSO
P1
P2
P3
WB
50
PfPKAr
60
PfCDPK1
30
Pf14-3-3I
% Inhibition
60
40
20
0
-20
-30
***
**
P1
P2
P3
P1
P2
P3
PfCDPK1
PfPKAr
c)
Pull down with Pf14-3-3I
DMSO
BV02
WB
Pf14-3-3I
PfPKAr
PfCDPK1
% Inhibition
100
50
0
***
***
PfCDPK1
PfPKAr

Figure 5

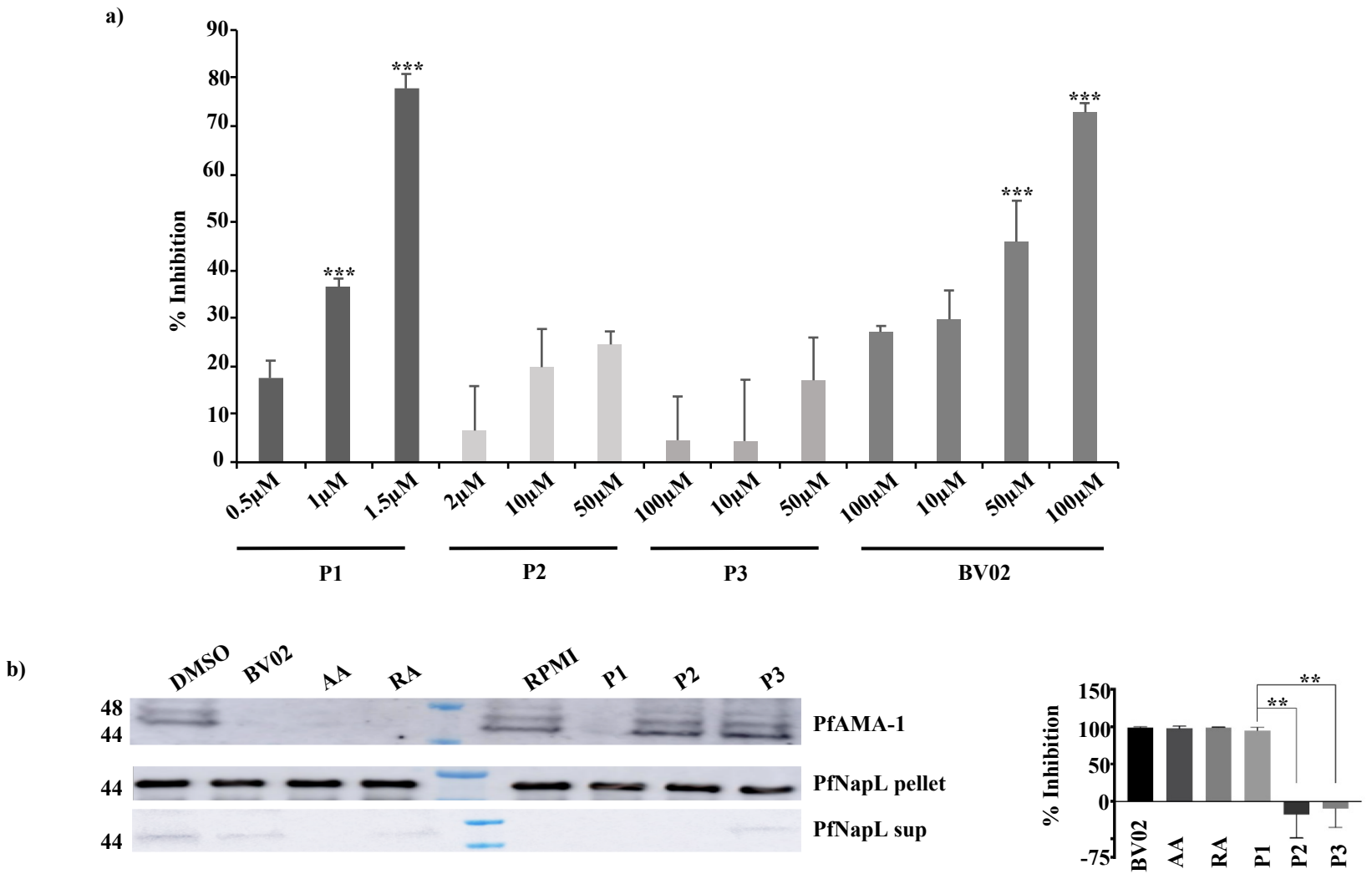
a)
% Inhibition
0
10
20
30
40
50
60
70
80
90
***
***
***
***
0.5µM
1µM
1.5µM
2µM
10µM
50µM
100µM
10µM
50µM
100µM
10µM
50µM
100µM
P1
P2
P3
BV02
b)
DMSO
BV02
AA
RA
RPMI
P1
P2
P3
48
44
44
44
PfAMA-1
PfNapL pellet
PfNapL sup
% Inhibition
150
100
50
0
-75
**
**
BV02
AA
RA
P1
P2
P3

Figure 6

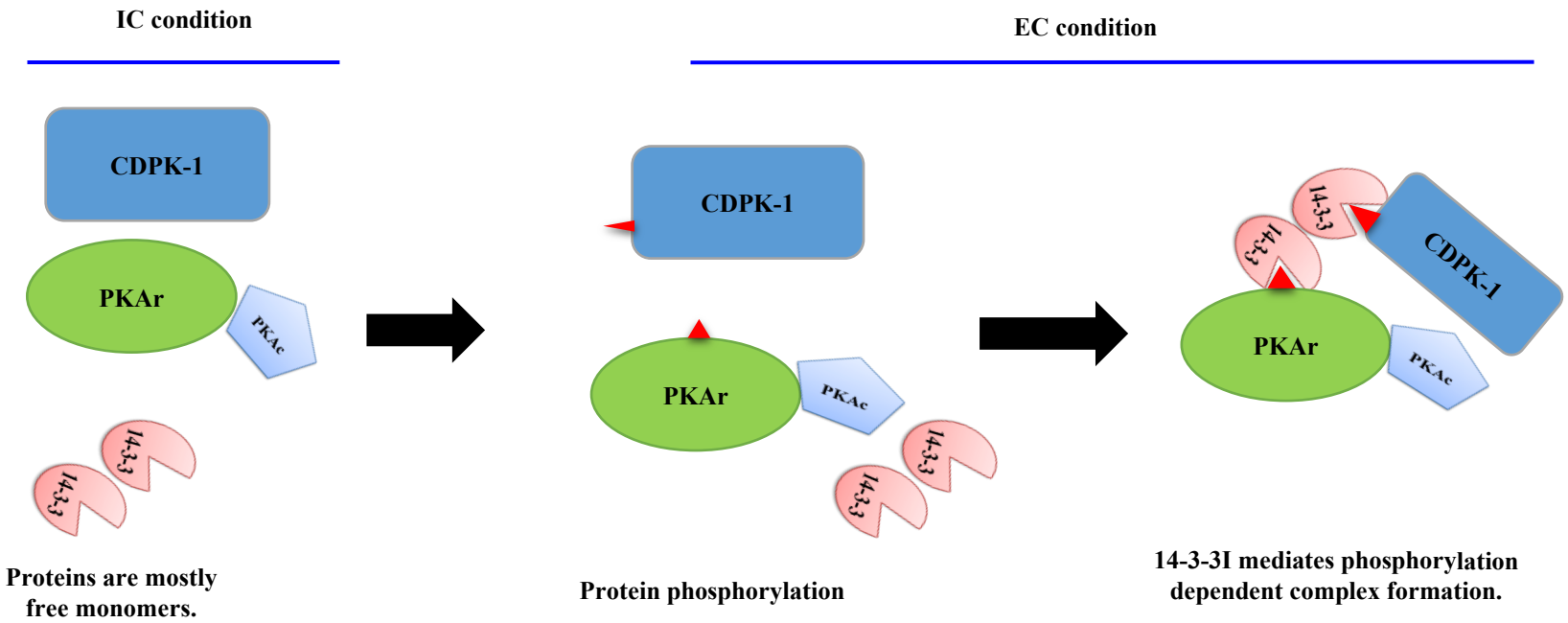
IC condition
EC condition
CDPK-1
PKAr
PKAc
14-3-3
14-3-3
CDPK-1
PKAr
PKAc
14-3-3
14-3-3
14-3-3
14-3-3
CDPK-1
PKAr
PKAc
Proteins are mostly free monomers.
Protein phosphorylation
14-3-3I mediates phosphorylation dependent complex formation.

Figure 7